New bounds on trilinear *R*-parity violation from lepton flavor violating observables

H. K. Dreiner,[1,*] K. Nickel,[1,†] F. Staub,[1,‡] and A. Vicente[2,§]

[1]*Bethe Center for Theoretical Physics & Physikalisches Institut der Universität Bonn, Nußallee 12, 53115 Bonn, Germany*
[2]*Laboratoire de Physique Théorique, CNRS–UMR 8627, Université de Paris-Sud 11, F-91405 Orsay Cedex, France*

(Received 3 May 2012; published 5 July 2012)

Many extensions of the leptonic sector of the minimal supersymmetric standard model (MSSM) are known, most of them leading to observable flavor violating effects. It has recently been shown that the 1-loop contributions to lepton flavor violating three-body decays $l_i \to 3l_j$ involving the Z^0 boson may be dominant, that is, much more important than the usual photonic penguins. Other processes like μ-e conversion in nuclei and flavor violating τ decays into mesons are also enhanced by the same effect. This is for instance also the case in the MSSM with trilinear R-parity violation. The aim of this work is to derive new bounds on the relevant combinations of R-parity violating couplings and to compare them with previous results in the literature. For heavy supersymmetric spectra the limits are improved by several orders of magnitude. For completeness, also constraints coming from flavor violating Z^0-decays and tree-level decay channels $l \to l_i l_j l_k$ are presented for a set of benchmark points.

DOI: 10.1103/PhysRevD.86.015003 PACS numbers: 12.60.Jv

I. INTRODUCTION

Supersymmetry (SUSY) is one of the most popular extensions of the standard model (SM) [1,2]. It provides a technical solution to the famous hierarchy problem [3–6] and contains the required ingredients to accommodate new physics [7].

However, no experimental evidence of supersymmetry has been found so far at the Large Hadron Collider (LHC) [8,9]. Direct searches, based mainly on the existence of missing transverse energy in the final state, have failed to find a signal that exceeds the SM background [10,11]. This should encourage the search for nonminimal supersymmetric scenarios with a departure from the usual supersymmetric signatures. Therefore, new strategies might be necessary, such as those required to look for trilinear R-parity violation (RpV) [12,13].

The nonobservation of lepton or baryon number violating processes in nature sets strong bounds on the trilinear R-parity violating couplings. Furthermore, some SM processes are also affected by the Introduction of these couplings, which allows us to set additional experimental limits. Many studies in this direction can be found; see for example [14–16].

The lepton flavor violating (LFV) decay $l_i \to 3l_j$, $i \neq j$, is a well-known process in supersymmetry. However, although detailed computations exist in the literature [17,18], some of its properties have been missed until very recently. The dominance of the photon mediation diagrams, only affected by Higgs mediation in the large $\tan\beta$ regime [19], has been part of the common lore for many years. This led to the simple relation

$$\mathrm{Br}(l_i \to 3l_j) \simeq \frac{\alpha}{3\pi}\left[\log\left(\frac{m_{l_i}^2}{m_{l_j}^2}\right) - \frac{11}{4}\right]\mathrm{Br}(l_i \to l_j\gamma), \quad (1)$$

which implies $\mathrm{Br}(l_i \to 3l_j) < \mathrm{Br}(l_i \to l_j\gamma)$. This is in fact true in the minimal supersymmetric standard model (MSSM) with lepton flavor violation. Contrary to this, it was recently pointed out that the Z^0 penguin, usually neglected or regarded as a subleading contribution, can induce a huge enhancement of the signal in extended models and lead to $\mathrm{Br}(l_i \to 3l_j) > \mathrm{Br}(l_i \to l_j\gamma)$ [20]. This implies that some LFV studies need to be revisited in order to take into account the constraining power of $l_i \to 3l_j$.

One of the extended scenarios where the Z^0 penguin enhancement is found is trilinear R-parity violation. The additional lepton number violating interactions, not present in the MSSM, induce a large 1-loop $\mathrm{Br}(l_i \to 3l_j)$. This increase has been unnoticed in the existing literature [21,22]. Furthermore, the same Z^0 penguins will also dominate the amplitudes for $\mu - e$ conversion in nuclei and $\tau \to l_j P^0$ decays (where P^0 is a pseudoscalar meson). We will use these observables to set new bounds on the combinations of trilinear couplings involved. Finally, for the sake of completeness, we will also cover the 1-loop decays $Z^0 \to l_i l_j$ and the tree-level decays $l_i \to 3l_j$ and $l_i \to l_j l_k l_k$ and refer to Ref. [23] for an exhaustive collection of bounds coming from tree-level decays involving mesons.

II. LEPTON FLAVOR VIOLATING OBSERVABLES IN *R*-PARITY VIOLATING SUSY

In this section we discuss how the flavor violating decays $l_i \to 3l_j$, $l_i \to l_j l_k l_k$, $Z^0 \to l_j l_k$ as well as $\mu - e$

*dreiner@th.physik.uni-bonn.de
†nickel@th.physik.uni-bonn.de
‡fnstaub@th.physik.uni-bonn.de
§avelino.vicente@th.u-psud.fr

conversion in nuclei and $\tau \to l_i P^0$ decays are induced in trilinear R-parity violating SUSY. Although the focus of this work is the impact of the Z^0 penguin on the 1-loop induced $l_i \to 3l_j$ decays and $\mu - e$ conversion in nuclei, we also study the loop induced decay $Z^0 \to l_j l_k$. In addition, the decays at tree-level are given for completeness in the Appendix.

A. Lepton flavor violating three-body decays: $l_i \to 3l_j$

We start our discussion with the leptonic three-body decay $l_i \to 3l_j$, since this process gives a clear understanding of the impact of the Z^0 penguin. The total width of the 1-loop induced $l_i \to 3l_j$ decay contains contributions from the photon penguin, the Higgs penguin, the Z^0 penguin, and box diagrams. For instance, the amplitudes for the important photon and Z^0 penguins can be written as

$$T_{\gamma\text{-penguin}} = \bar{u}_i(p_1)[q^2\gamma_\mu(A_1^L P_L + A_1^R P_R) + im_{l_j}\sigma_{\mu\nu}q^\nu(A_2^L P_L + A_2^R P_R)]u_j(p) \times \frac{e^2}{q^2}\bar{u}_i(p_2)\gamma^\mu v_i(p_3) - (p_1 \leftrightarrow p_2), \quad (2)$$

$$T_{Z^0\text{-penguin}} = \frac{1}{m_Z^2}\bar{u}_i(p_1)[\gamma_\mu(F_L P_L + F_R P_R)]u_j(p)\bar{u}_i(p_2)[\gamma^\mu(Z_L^{(l)} P_L + Z_R^{(l)} P_R)]v_i(p_3) - (p_1 \leftrightarrow p_2). \quad (3)$$

Here $A_{1,2}^{L,R}$ and $F_{L,R}$ represent the 1-loop form factors induced by the photon and Z^0-boson exchange, respectively, and $Z_{L,R}^{(l)}$ are the standard Z^0-boson couplings to the leptons. The long expressions for the scalar penguins and boxes can be parametrized by the operators $B_{L,R}^I$ (with $I = 1, \ldots, 4$). The total width $\Gamma \equiv \Gamma(l_i^- \to l_j^- l_j^- l_j^+)$ is obtained as [17,18]

$$\begin{aligned}\Gamma = \frac{e^4}{512\pi^3} m_{l_i}^5 [&|A_1^L|^2 + |A_1^R|^2 - 2(A_1^L A_2^{R*} + A_2^L A_1^{R*} + \text{H.c.}) + (|A_2^L|^2 + |A_2^R|^2)\left(\frac{16}{3}\log\frac{m_{l_i}}{m_{l_j}} - \frac{22}{3}\right) + \frac{1}{6}(|B_1^L|^2 + |B_1^R|^2) \\ &+ \frac{1}{3}(|\hat{B}_2^L|^2 + |\hat{B}_2^R|^2) + \frac{1}{24}(|\hat{B}_3^L|^2 + |\hat{B}_3^R|^2) + 6(|B_4^L|^2 + |B_4^R|^2) - \frac{1}{2}(\hat{B}_3^L B_4^{L*} + \hat{B}_3^R B_4^{R*} + \text{H.c.}) \\ &+ \frac{1}{3}(A_1^L B_1^{L*} + A_1^R B_1^{R*} + A_1^L \hat{B}_2^{L*} + A_1^R \hat{B}_2^{R*} + \text{H.c.}) - \frac{2}{3}(A_2^R B_1^{L*} + A_2^L B_1^{R*} + A_2^L \hat{B}_2^{R*} + A_2^R \hat{B}_2^{L*} + \text{H.c.}) \\ &+ \frac{1}{3}\{2(|F_{LL}|^2 + |F_{RR}|^2) + |F_{LR}|^2 + |F_{RL}|^2 + (B_1^L F_{LL}^* + B_1^R F_{RR}^* + \hat{B}_2^L F_{LR}^* + \hat{B}_2^R F_{RL}^* + \text{H.c.}) \\ &+ 2(A_1^L F_{LL}^* + A_1^R F_{RR}^* + \text{H.c.}) + (A_1^L F_{LR}^* + A_1^R F_{RL}^* + \text{H.c.}) - 4(A_2^R F_{LL}^* + A_2^L F_{RR}^* + \text{H.c.}) - 2(A_2^L F_{RL}^* + A_2^R F_{LR}^* + \text{H.c.})\}].\end{aligned} \quad (4)$$

Here, F_{XY} are functions of F_L and F_R, and the Higgs and box contributions are combined into $\hat{B}$. Exact definitions can be found in [18]. We do not repeat them here for the sake of brevity. Finally, $\text{Br}(l_i \to l_j\gamma)$, $i \neq j$, is completely determined by the same form factors A_2^L and A_2^R

$$\text{Br}(l_i \to l_j\gamma) = \frac{e^2}{16\pi} m_{l_i}^5 (|A_2^L|^2 + |A_2^R|^2). \quad (5)$$

For many years the decay $l_i \to 3l_j$ has been believed to be dominated by photon exchange, with large Higgs contributions in the large $\tan\beta$ regime [19]. This has recently been challenged in Ref. [20], where it was shown that many simple extensions of the leptonic sector can lead to large enhancements for the Z^0 boson contributions. This may lead to Z^0-penguin dominated scenarios where $\text{Br}(l_i \to 3l_j) > \text{Br}(l_i \to l_j\gamma)$. In fact, this can be understood from simple dimensional arguments. As shown in Eq. (4), the decay width is proportional to $m_{l_i}^5$, so both A and F form factors must have dimensions of inverse mass squared. Thus we only have to determine what is the mass scale for each case. First, the vanishing mass of the photon implies that the only mass scale involved in the A form factors is m_{SUSY}. On the other hand, the mass scale of the F form factor is set by m_Z, the Z^0 boson mass. Therefore, we conclude that $A \sim m_{\text{SUSY}}^{-2}$ and $F \sim m_Z^{-2}$. This fact can be checked analytically in the complete expressions given in Refs. [17,18]. With $m_Z^2 \ll m_{\text{SUSY}}^2$ the Z^0 penguin can, in principle, be even more important than the photonic one.

However, in the case of the MSSM the photonic penguin is found to be numerically dominant [18]. This is caused by a subtle cancellation among the different Z^0 boson diagrams [20], which strongly suppresses their contribution to the amplitude of the process. We note that a similar behavior was found in Ref. [24] for the decay $B \to X_s l^+ l^-$.

However, this cancellation can easily be spoiled by two effects, either (1) extended particle content, or (2) new interactions in the lepton sector. Trilinear R-parity violation is a simple example of the second case. The additional interactions of the leptons lead to new loop diagrams including charged leptons, which do not suffer from the same cancellation as the wino does and induce a large increase in the $l_i \to 3l_j$ signal; cf. the Z^0 mediated diagrams in Fig. 1. It is the object of this paper to study how this increase, together with the current experimental

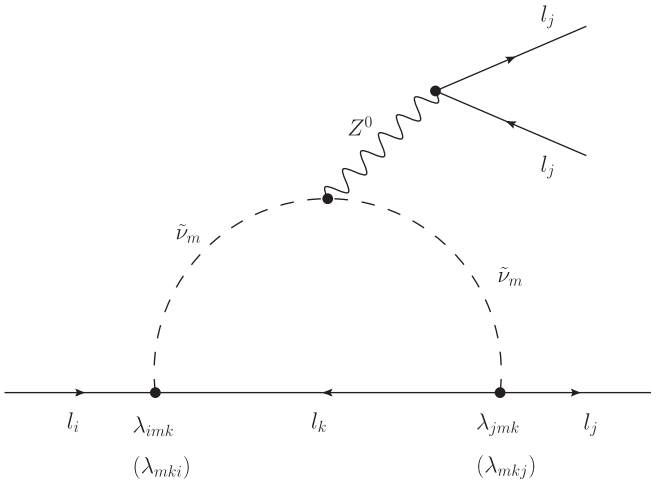

FIG. 1. One-loop induced $l_i \to 3l_j$ decays. As shown in brackets, there are two possible combinations of λ couplings: $\lambda_{jmk}\lambda_{imk}$ and $\lambda_{mkj}\lambda_{mki}$. Moreover, we remind the reader that the λ couplings are antisymmetric in the first two indices. Similar diagrams with the Z^0 boson line attached to the lepton lines are also possible.

bounds, constrains the relevant parameter space. We will also shortly comment on the impact of possible future improvements on the experimental limit for this observable [25].

So far, we have not mentioned decays of the form $l_i \to l_j l_k l_k$ with different generations of leptons in the final states. The reason is that these decays will always be less constraining than $l_i \to 3l_j$ because of combinatorical factors that lead to $\mathrm{Br}(l_i \to l_j) > \mathrm{Br}(l_i \to l_j l_k l_k)$ [26].

B. $\mu - e$ conversion

Let us now discuss $\mu - e$ conversion in nuclei. This process is also mediated by photonic, Z^0, and Higgs penguins as well as box diagrams [27]. The Z^0 contributions are given by the same diagram as shown in Fig. 1 with the two external leptons attached to the Z^0 replaced by quarks. The conversion rate can be expressed as [27]

$$\begin{aligned}\mathrm{Cr}(\mu - e, \text{ Nucleus}) &= \frac{1}{\Gamma_{\text{capt}}} \frac{p_e E_e m_\mu^3 G_F^2 \alpha^3 Z_{\text{eff}}^4 F_p^2}{8\pi^2 Z} \cdot (|(Z+N)^2(g_{LV}^{(0)} + g_{LS}^{(0)}) \\ &\quad + (Z-N)(g_{LV}^{(1)} + g_{LS}^{(1)})|^2 + L \leftrightarrow R). \end{aligned} \tag{6}$$

Here, Z and N are the number of protons and neutrons in the nucleus, Z_{eff} is an effective charge, F_p is the nuclear matrix element, and Γ_{capt} denotes the total muon capture rate. The different contributions $g_{XY}^{(J)}$ ($X = L, R$, $Y = V, S$, $J = 0, 1$) are functions of the same form factors A and F already introduced in Eqs. (2) and (3) as well as of scalar penguins and box diagrams. For a detailed discussion we refer to Ref. [27].

Similarly, the decays $\tau \to l_i P^0$ get contributions from Z^0 mediated diagrams, which lead to the corresponding F form factors, and from pseudoscalar (A^0) mediated diagrams [28]. As for $\mu - e$ conversion in nuclei, one expects that the Z^0 penguins dominate. Furthermore, it turns out that $\mu - e$ conversion in nuclei and $\tau \to l_i P^0$ are even more constraining than $l_i \to 3l_j$. This is mainly due to the very good existing experimental limits [29–31]. In addition, there are also very good experimental perspectives, with plans for a sensitivity for $\mu - e$ conversion rates as low as 10^{-18}–10^{-16} [32,33]. A detailed comparison of the importance of the different observables is given in Sec. IV.

C. Lepton flavor violating Z^0 decays

As already mentioned, we also present here results for the lepton flavor violating Z^0 decays. These have been discussed in the context of trilinear R-parity violation in Refs. [34,35]. These decays are triggered by diagrams like the one given in Fig. 1 but without the two leptons attached to the Z^0 boson. The branching ratio can be expressed as [36]

$$\begin{aligned}\mathrm{Br}(Z^0 \to l_i l_j) = \frac{1}{\Gamma_Z} \frac{1}{48\pi m_z} \Big[& 2(|a_1|^2 + |a_2|^2) m_z^2 \\ & + \frac{1}{4}(|a_3|^2 + |a_4|^2) m_z^4 \Big]. \end{aligned} \tag{7}$$

There is only an explicit suppression by the SUSY scale for the contributions a_3 and a_4, but a_1 and a_2 are dimensionless. This observable has been discussed in the context of a SUSY $SO(10)$ model in [36]. Because of this dependence on the different scales, the authors have observed in the considered $SO(10)$ model that $\mathrm{Br}(Z^0 \to \tau\mu)$ actually increases with increasing universal scalar mass m_0, until it saturates. However, the overall impact of this observable was found to be rather small because of the weak experimental limits. We note that a similar behavior was found in [35].

III. TRILINEAR R-PARITY VIOLATION

We consider in this work the impact of the Z^0 penguins in the MSSM extended by the lepton number violating terms [12,13]

$$W_{\not R} = \tfrac{1}{2}\lambda_{ijk}\hat{L}_i\hat{L}_j\hat{E}_k^c + \lambda'_{ijk}\hat{L}_i\hat{Q}_j\hat{D}_k^c. \tag{8}$$

In the following, we use the acronyms LLE and LQD for the $\hat{L}_i\hat{L}_j\hat{E}_k^c$ and $\hat{L}_i\hat{Q}_j\hat{D}_k^c$ couplings, respectively. Bounds for these trilinear couplings have been set so far by using not only lepton flavor violating decays but also $\mu - e$ conversion in nuclei or cosmological observations. This led to limits on individual couplings or specific products of couplings [14–16,23,37–40]. However, all studies dealing with $\mathrm{Br}(l_i \to l_j l_k l_l)$ have so far neglected all contributions but the photonic penguins. Also the bounds from rare Z^0 decays in case of trilinear R-parity violation have not been presented in the literature so far.

Before we discuss the new bounds that arise if one performs the full calculation including all contributions, we comment shortly on the bilinear R-parity violating term that was skipped in Eq. (8). It is well known that the trilinear couplings will induce also a term $\kappa_i \hat{L}_i \hat{H}_u$ during the renormalization group equation evaluation [13,41]. This term, as well as the corresponding soft-breaking terms $B_{\kappa_i} H_u \tilde{l}_i$ and $m^2_{H_d l} \tilde{l}^*_i H_d$, leads already at tree level to a mixing between standard model and supersymmetric states. In addition, they generate small vacuum expectation values (VEVs) for the sneutrinos.[1] However, the values of κ_i are restricted by neutrino data and the size of the additional VEVs by electroweak precision data. Therefore, the impact of bilinear R-parity violation and the related couplings on the lepton flavor violating decays considered here are in general subdominant and numerically negligible [20]. The only exception can be found when a large lepton-chargino mixing, which can open new tree-level channels, is induced. However, also these contributions are suppressed by the SUSY scale and might only be relevant for light spectra [43].

IV. NUMERICAL ANALYSIS

A. Setup

The numerical analysis has been performed by means of the Fortran package SPHENO [44,45] using the Mathematica interface provided by SARAH [46–48].

The Fortran code generated by SARAH to calculate $l_i \to 3 l_j$ and $l_i \to l_j \gamma$ is based on the generalization of the formulas given in Ref. [18]. The routines for $\mu - e$ conversion and $\tau \to l_i P^0$ are based on Refs. [27,28], respectively. The generic expressions for the rare Z^0 decays have been calculated with FEYNARTS and FORMCALC [49,50] and have been compared with the formulas of Ref. [36]: while we agree with the vertex correction, our results for the wave function contributions are smaller by an overall factor of 2. The output of the SPHENO code for $\mu - e$ conversion in nuclei, $\tau \to l_i P^0$ decays, and lepton flavor violating Z^0 decays will become a new public feature of SARAH 3.1.0.

We want to stress that in case of the three-body decays or $\mu - e$ conversion in nuclei our computation includes not only the photonic and Z^0 penguins but also the contributions from Higgs penguins and box diagrams. Finally, SARAH writes the routines to calculate all three-body decays of fermions at tree level, which were used to obtain the results given in the Appendix.

To disentangle the effect of the renormalization group evaluation, we have first calculated the MSSM parameters at the electroweak scale for three benchmark points given in Ref. [51]. These points are called BP1—BP3 in the following. In addition, we have included a constrained MSSM scenario, which leads to sneutrino masses of $\sim$100 GeV (point BP0). Although this point leads to a SUSY spectrum already ruled out by LHC searches, it is presented here to compare the obtained results with the bounds previously given in the literature. Even BP1 might already be borderline, especially as long as R-parity violating effects are small. However, we have included it here also to close the gap between the old studies in the literature and the points BP2 and BP3 with a heavy spectrum that satisfy all recent collider bounds. The input parameters as well as some relevant masses are given in Table I. In the table we focused on the relevant masses for the discussion and skipped those that play a negligible role in the calculation of the constraints. As expected, the main result can in general be obtained from the diagram shown in Fig. 1. Similar diagrams with neutralinos or charginos give smaller contributions.

TABLE I. Input parameters as well as relevant SUSY masses for benchmark points BP0–BP3. BP1–BP3 correspond to those points of Ref. [51], as indicated in the second row. BP0 is included for comparison with earlier results in the literature. All masses are given in GeV.

	BP0	BP1	BP2	BP3
[51]		10.1.1	10.4.1	40.2.5
Input				
m_0 [GeV]	100	125	750	750
$M_{1/2}$ [GeV]	100	500	350	650
$\tan(\beta)$	10	10	10	40
sign(μ)	+	+	+	+
A_0 [GeV]	0	0	0	−500
Masses				
$\tilde{d}_R$, $\tilde{s}_R$	257.8	1017.5	1497.0	1483.5
$\tilde{d}_L$, $\tilde{s}_L$	261.0	1020.9	1503.8	1532.9
$\tilde{b}_1$	240.7	975.1	1434.2	1285.6
$\tilde{b}_2$	269.8	1065.9	1570.0	1364.7
$\tilde{u}_R$, $\tilde{c}_R$	254.7	1024.3	1509.7	1477.8
$\tilde{u}_L$, $\tilde{c}_L$	257.8	1063.1	1568.1	1531.0
$\tilde{t}_1$	190.3	812.1	1208.8	1095.0
$\tilde{t}_2$	331.8	1021.2	1466.1	1333.0
$\tilde{e}_R$, $\tilde{\mu}_R$	115.2	229.7	450.2	788.6
$\tilde{e}_L$, $\tilde{\mu}_L$	129.9	361.2	610.3	864.9
$\tilde{\tau}_1$	107.8	222.1	442.5	601.8
$\tilde{\tau}_2$	134.8	362.5	611.1	801.6
$\tilde{\nu}_e$, $\tilde{\nu}_\mu$	102.0	352.2	605.7	860.6
$\tilde{\nu}_\tau$	101.4	351.0	603.5	787.0

After the calculation of the MSSM spectrum, we switched on the different combinations of the RpV couplings that can open flavor violating decay or transition channels and calculated the different observables at tree and 1-loop level. The tree-level results are given in the Appendix.

In the determination of the bounds we have used the most recent experimental upper limits given in Table II.

[1]For these and other aspects of bilinear R-parity violation and neutrino mass generation see Ref. [42] and references therein.

TABLE II. Current experimental upper limits on flavor violating two- and three-body decays [$\mathrm{Br}(l_i \to l_j\gamma)/\mathrm{Br}(l_i \to 3l_j)$], flavor violating Z^0 decays [$\mathrm{Br}(Z^0 \to l_i l_j)$], $\mu - e$ conversion rate [$\mathrm{Cr}(\mu - e, X)$], and semileptonic, flavor violating τ decays ($\tau \to l_i P^0$) [29–31,52,53].

$\mathrm{Br}(\mu \to e\gamma)$	2.4×10^{-12}	$\mathrm{Br}(\tau \to e\gamma)$	3.3×10^{-8}	$\mathrm{Br}(\tau \to \mu\gamma)$	4.4×10^{-8}
$\mathrm{Br}(\mu \to 3e)$	1.0×10^{-12}	$\mathrm{Br}(\tau \to 3\mu)$	2.7×10^{-8}	$\mathrm{Br}(\tau \to 3\mu)$	2.1×10^{-8}
$\mathrm{Br}(Z^0 \to e\mu)$	1.7×10^{-6}	$\mathrm{Br}(Z^0 \to e\tau)$	9.8×10^{-6}	$\mathrm{Br}(Z^0 \to \mu\tau)$	1.2×10^{-5}
$\mathrm{Cr}(\mu - e, \mathrm{Pb})$	4.6×10^{-11}	$\mathrm{Cr}(\mu - e, \mathrm{Ti})$	6.1×10^{-13}	$\mathrm{Cr}(\mu - e, \mathrm{Au})$	7.0×10^{-13}
$\mathrm{Br}(\tau \to e\pi^0)$	8.0×10^{-8}	$\mathrm{Br}(\tau \to e\eta)$	9.2×10^{-8}	$\mathrm{Br}(\tau \to e\eta')$	1.6×10^{-7}
$\mathrm{Br}(\tau \to \mu\pi^0)$	1.1×10^{-7}	$\mathrm{Br}(\tau \to \mu\eta)$	6.5×10^{-8}	$\mathrm{Br}(\tau \to \mu\eta')$	1.3×10^{-7}

For the 1-loop induced decays, the limits would not be improved if we also took into account observables with two different generations of leptons in the final state. This is due to the fact that $\tau^- \to e^+\mu^-\mu^-$ and $\tau^- \to \mu^+ e^- e^-$ would only be triggered by box diagrams, which are in general suppressed with respect to the penguins. In addition, the branching ratios for decays like $\tau^- \to e^-\mu^+\mu^-$ will always be smaller than those for a single flavor final state. The reason for this can be found in the relative factors of the Z^0 and photon contributions in the corresponding partial widths. They always lead to $\mathrm{Br}(l_i \to 3l_j) > \mathrm{Br}(l_i \to l_j l_j l_k)$ $(j \neq k)$; see Ref. [26].

B. Results for 1-loop induced observables

The focus in this section is on combinations of λ and λ', which do not open flavor violating tree-level decay channels for the leptons if there is not any other source of lepton flavor violation.[2] For those couplings all possible final states at tree level are kinematically forbidden but other decay channels are induced at 1-loop. The results for all other pairs of trilinear couplings that do open tree-level channels are given for completeness in the Appendix.

Before we present the updated bounds derived in our work, we briefly comment on earlier results. In Ref. [22] the old Muon to Electron and Gamma (MEG) limit for $\mathrm{Br}(\mu \to e\gamma) < 1.2 \times 10^{-11}$ has been used, and the limits $|\lambda^*_{132} \cdot \lambda_{232}| < 2.3 \times 10^{-4}$ and $|\lambda^*_{231} \cdot \lambda_{232}| < 8.2 \times 10^{-5}$ were obtained. We have explicitly checked with our code that, using the same experimental limit, one finds 2.1×10^{-4} and 8.0×10^{-5}, respectively, for the same combinations of λ couplings. This is in rather good agreement and gives an idea of the expected theoretical uncertainty.

It has also been shown in Ref. [22] that $\mu \to 3e$ can be more constraining than $\mu \to e\gamma$. However, this result was not based on the inclusion of the Z^0 penguins but instead on polarization effects. They set the limits $|\lambda^*_{132} \cdot \lambda_{232}| < 7.1 \times 10^{-5}$ and $|\lambda^*_{231} \cdot \lambda_{232}| < 4.5 \times 10^{-5}$. These bounds can already be reached just by including the Z^0 penguins, without the necessity to consider polarization effects. In fact, for the spectrum of BP0 we get

$$|\lambda^*_{132} \cdot \lambda_{232}| < 6.8 \times 10^{-5}, \quad |\lambda^*_{231} \cdot \lambda_{232}| < 4.6 \times 10^{-5}. \quad (9)$$

All the bounds evaluated using the spectrum of the benchmark point BP0 are collected in Table III. One can easily see that the limits from Z^0 decays are very weak but all other observables provide bounds of the same order for most combinations of couplings. However, as already mentioned in the Introduction, both $l_i \to l_j\gamma$ and the photonic contributions to $l_i \to 3l_j$ and $\mu - e$ conversion in nuclei scale as m^{-4}_{SUSY} [20]. Hence, if one includes only these contributions, all bounds are much weaker for a heavier spectrum as in BP1 to BP3. In contrast, as shown in [20], $l_i \to 3l_j$ is much less sensitive to the SUSY scale as soon as the Z^0 penguins dominate: the Z^0 penguins are increased by a factor $m^4_{\mathrm{SUSY}}/m^4_{\mathrm{Z}}$ in comparison to the photonic contributions. The same happens for the Z^0 contributions to $\mu - e$ conversion in nuclei and $\tau \to l_i P^0$ decays. To show this different behavior, we depict in Fig. 2 the dependence of $\mathrm{Br}(\mu \to e\gamma)$ and $\mathrm{Br}(\mu \to 3e)$ for BP0 and BP2 on one combination of LLE couplings. While for BP0 $\mathrm{Br}(\mu \to e\gamma) > \mathrm{Br}(\mu \to 3e)$ holds, the order is changed for BP2 because $\mathrm{Br}(\mu \to e\gamma)$ is shifted to the right while $\mathrm{Br}(\mu \to 3e)$ has only slightly moved.

TABLE III. New limits using our calculation evaluated at the benchmark point BP0 on different combinations of LLE and LQD operators derived from low energy precision observables and the experimental limits given in Table II.

Coupling	$l_i \to l_j\gamma$	$l_i \to 3l_j$	$\tau \to lP/\mu - e$	$Z \to l_i l_j$
$\lvert\lambda^*_{123}\lambda_{133}\rvert$	3.2×10^{-2}	4.8×10^{-2}	2.0	2.8
$\lvert\lambda^*_{123}\lambda_{233}\rvert$	2.7×10^{-2}	5.3×10^{-2}	4.9	7.9
$\lvert\lambda^*_{132}\lambda_{232}\rvert$	9.1×10^{-5}	6.8×10^{-5}	1.5×10^{-5}	3.5
$\lvert\lambda^*_{133}\lambda_{233}\rvert$	4.4×10^{-5}	1.2×10^{-4}	2.6×10^{-5}	3.3
$\lvert\lambda^*_{231}\lambda_{232}\rvert$	3.5×10^{-5}	4.6×10^{-5}	7.7×10^{-6}	2.7
$\lvert\lambda'^*_{122}\lambda'_{222}\rvert$	1.5×10^{-5}	7.4×10^{-5}	1.9×10^{-5}	1.3×10^{-1}
$\lvert\lambda'^*_{123}\lambda'_{223}\rvert$	1.5×10^{-5}	7.4×10^{-5}	1.9×10^{-5}	1.3×10^{-1}
$\lvert\lambda'^*_{132}\lambda'_{232}\rvert$	1.5×10^{-5}	7.1×10^{-5}	1.9×10^{-5}	1.1×10^{-1}
$\lvert\lambda'^*_{133}\lambda'_{233}\rvert$	1.5×10^{-5}	7.1×10^{-5}	1.8×10^{-5}	1.1×10^{-1}
$\lvert\lambda'^*_{133}\lambda'_{333}\rvert$	4.2×10^{-3}	2.5×10^{-2}	5.2×10^{-2}	2.7×10^{-1}
$\lvert\lambda'^*_{233}\lambda'_{333}\rvert$	4.9×10^{-3}	2.7×10^{-2}	6.1×10^{-2}	3.0×10^{-1}

[2]Pairs of λ discussed in this section enable decays $l_i \to l_j 2\nu$ at tree level. However, the experimental limits are very weak and thus the resulting bounds on the values of λ's are not competitive with the ones discussed in this work.

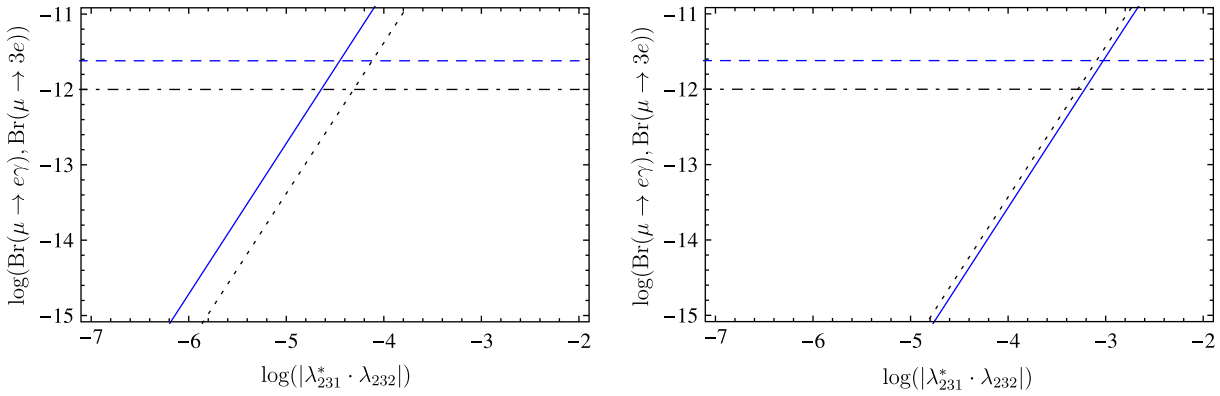

FIG. 2 (color online). $\mathrm{Br}(\mu \to e\gamma)$ (solid line) and $\mathrm{Br}(\mu \to 3e)$ (dotted line) for BP0 (left) and BP2 (right). The current upper experimental bounds are given by the dashed [$\mathrm{Br}(\mu \to e\gamma)$] and dot-dashed ($\mathrm{Br}(\mu \to 3e)$) lines.

Thus indeed the bounds from $l_i \to 3l_j$ are less sensitive to an increase in the SUSY mass scale. And using $\mathrm{Br}(\mu \to 3e)$, it is possible to derive bounds on the couplings for the points BP1—BP3 which are of the same order as those given in Eq. (9) for a light SUSY spectrum. This can be seen in Tables IV, V, and VI, where we give the limits of all combinations of trilinear couplings, which do not open channels for leptonic flavor violating processes at tree level.[3]

Thus as discussed above, the bounds coming from observables that involve Z^0 penguin diagrams depend only very mildly on the SUSY point. In fact, some bounds even get improved slightly with a heavier mass spectrum. This is more pronounced in case of LQD couplings. In particular, BP2 and BP3 are a bit more restrictive than BP1 and BP0. The reason for this can be found in the wave function contributions to the Z^0 penguins involving the loop function B_1 [18]

$$B_1(m_q^2, m_{\tilde{q}}^2) = -\frac{1}{2} + \frac{1}{2}\log(m_{\tilde{q}}^2) - \frac{m_q^2 - m_{\tilde{q}}^2 + 2m_1^2 \log(\frac{m_{\tilde{q}}^2}{m_q^2})}{4(m_q^2 - m_{\tilde{q}}^2)^2} \tag{10}$$

with quark mass m_q and squark mass $m_{\tilde{q}}$. Hence, these contributions grow logarithmically with the scalar masses in the loop.

The combinations $|\lambda^*_{123}\lambda_{233}|$, $|\lambda^*_{123}\lambda_{133}|$, $|\lambda'^*_{133}\lambda'_{333}|$, and $|\lambda'^*_{233}\lambda'_{333}|$ are less constrained than the other $|\lambda^*\lambda|$ or $|\lambda'^*\lambda'|$ combinations because they induce τ decays while all other combinations contribute to μ decays. Nevertheless, these combinations show in general the same qualitative behavior when the different benchmark points are compared.

[3]With lepton flavor violating decays we refer only to processes with three charged leptons in the final states. The couplings will open decays $l \to l_i \nu_j \nu_k$, but those are experimentally unconstrained.

TABLE IV. Limits for the benchmark point BP1 on different combinations of LLE and LQD operators derived from low energy precision observables and the experimental limits given in Table II.

Coupling	$l_i \to l_j\gamma$	$l_i \to 3l_j$	$\tau \to l_iP/\mu - e$	$Z^0 \to l_il_j$
$\lvert\lambda^*_{123}\lambda_{133}\rvert$	5.5×10^{-1}	4.8×10^{-1}	3.4×10^{1}	4.5
$\lvert\lambda^*_{123}\lambda_{233}\rvert$	4.8×10^{-1}	5.4×10^{-1}	5.3	1.3×10^{1}
$\lvert\lambda^*_{132}\lambda_{232}\rvert$	2.3×10^{-3}	8.2×10^{-4}	1.6×10^{-4}	5.8
$\lvert\lambda^*_{133}\lambda_{233}\rvert$	5.6×10^{-4}	1.1×10^{-3}	2.2×10^{-4}	5.4
$\lvert\lambda^*_{231}\lambda_{232}\rvert$	3.8×10^{-4}	4.1×10^{-4}	1.2×10^{-4}	9.7
$\lvert\lambda'^*_{122}\lambda'_{222}\rvert$	1.2×10^{-4}	5.0×10^{-5}	1.0×10^{-5}	1.8
$\lvert\lambda'^*_{123}\lambda'_{223}\rvert$	1.2×10^{-4}	5.0×10^{-5}	1.0×10^{-5}	1.8
$\lvert\lambda'^*_{132}\lambda'_{232}\rvert$	1.3×10^{-4}	5.3×10^{-5}	1.1×10^{-5}	8.1×10^{-1}
$\lvert\lambda'^*_{133}\lambda'_{233}\rvert$	1.3×10^{-4}	5.3×10^{-5}	1.1×10^{-5}	8.1×10^{-1}
$\lvert\lambda'^*_{133}\lambda'_{333}\rvert$	3.3×10^{-2}	2.1×10^{-2}	3.7×10^{-2}	1.9
$\lvert\lambda'^*_{233}\lambda'_{333}\rvert$	3.8×10^{-2}	1.8×10^{-2}	4.3×10^{-2}	2.2

TABLE V. Limits for BP2 on different combinations of LLE and LQD operators derived from low energy precision observables and the experimental limits given in Table II.

Coupling	$l_i \to l_j\gamma$	$l_i \to 3l_j$	$\tau \to l_iP/\mu - e$	$Z^0 \to l_il_j$
$\lvert\lambda^*_{123}\lambda_{133}\rvert$	1.8×10^{1}	1.2	8.3×10^{1}	1.4×10^{1}
$\lvert\lambda^*_{123}\lambda_{233}\rvert$	1.3×10^{1}	1.4	5.9	$4. \times 10^{1}$
$\lvert\lambda^*_{132}\lambda_{232}\rvert$	2.4×10^{-1}	2.2×10^{-3}	4.2×10^{-4}	1.7×10^{1}
$\lvert\lambda^*_{133}\lambda_{233}\rvert$	1.7×10^{-3}	3.0×10^{-3}	6.1×10^{-4}	1.7×10^{1}
$\lvert\lambda^*_{231}\lambda_{232}\rvert$	9.5×10^{-4}	5.2×10^{-4}	2.4×10^{-4}	2.3×10^{1}
$\lvert\lambda'^*_{122}\lambda'_{222}\rvert$	4.5×10^{-4}	4.3×10^{-5}	8.8×10^{-6}	7.5×10^{-1}
$\lvert\lambda'^*_{123}\lambda'_{223}\rvert$	4.6×10^{-4}	4.3×10^{-5}	9.0×10^{-6}	7.5×10^{-1}
$\lvert\lambda'^*_{132}\lambda'_{232}\rvert$	4.9×10^{-4}	4.5×10^{-5}	9.3×10^{-6}	1.4
$\lvert\lambda'^*_{133}\lambda'_{233}\rvert$	4.9×10^{-4}	4.5×10^{-5}	9.3×10^{-6}	1.4
$\lvert\lambda'^*_{133}\lambda'_{333}\rvert$	1.3×10^{-1}	1.8×10^{-2}	3.1×10^{-2}	3.3
$\lvert\lambda'^*_{233}\lambda'_{333}\rvert$	1.5×10^{-1}	1.6×10^{-2}	3.6×10^{-2}	3.6

TABLE VI. Limits for BP3 on different combinations of LLE and LQD operators derived from low energy precision observables and the experimental limits given in Table II.

Coupling	$l_i \to l_j\gamma$	$l_i \to 3l_j$	$\tau \to l_iP/\mu - e$	$Z^0 \to l_il_j$
$\lvert\lambda^*_{123}\lambda_{133}\rvert$	1.2×10^{1}	2.4	6.9	2.0×10^{1}
$\lvert\lambda^*_{123}\lambda_{233}\rvert$	1.2×10^{1}	2.8	2.1×10^{-1}	5.7×10^{1}
$\lvert\lambda^*_{132}\lambda_{232}\rvert$	3.4×10^{-3}	3.3×10^{-3}	6.5×10^{-4}	6.1×10^{1}
$\lvert\lambda^*_{133}\lambda_{233}\rvert$	1.9×10^{-3}	4.5×10^{-3}	9.2×10^{-4}	2.8×10^{1}
$\lvert\lambda^*_{231}\lambda_{232}\rvert$	3.1×10^{-3}	4.7×10^{-4}	1.3×10^{-4}	3.6×10^{1}
$\lvert\lambda'^*_{122}\lambda'_{222}\rvert$	$3. \times 10^{-4}$	4.3×10^{-5}	9.0×10^{-6}	8.9×10^{-1}
$\lvert\lambda'^*_{123}\lambda'_{223}\rvert$	3.3×10^{-4}	4.4×10^{-5}	9.0×10^{-6}	8.9×10^{-1}
$\lvert\lambda'^*_{132}\lambda'_{232}\rvert$	3.4×10^{-4}	4.7×10^{-5}	9.1×10^{-6}	6.7
$\lvert\lambda'^*_{133}\lambda'_{233}\rvert$	3.8×10^{-4}	4.7×10^{-5}	9.7×10^{-6}	8.6
$\lvert\lambda'^*_{133}\lambda'_{333}\rvert$	8.7×10^{-2}	1.8×10^{-2}	2.2×10^{-2}	2.1×10^{1}
$\lvert\lambda'^*_{233}\lambda'_{333}\rvert$	9.8×10^{-2}	1.6×10^{-2}	3.8×10^{-2}	2.3×10^{1}

A final comment about the lepton flavor violating three-body decays: while the derived bounds on $|\lambda^*_{132}\lambda_{232}|$ and $|\lambda^*_{133}\lambda_{233}|$ are of the same size, $|\lambda^*_{231}\lambda_{232}|$ is always a bit more constrained. The difference between these contributions is that for the first two combinations the charged lepton can be right-handed while for the third case the lepton has to be left-handed and has therefore a larger coupling to the Z^0 boson.

$\mu - e$ conversion in nuclei in the context of trilinear R-parity violation was also studied in Ref. [22]. The limit obtained for instance for $|\lambda^*_{132}\lambda_{232}|$ was 1.3×10^{-5}. This bound is based on the same experimental limit of $\mathrm{Cr}(\mu - e, \mathrm{Ti})$ given in Table II for which we get nearly the same value as for gold nuclei, namely $|\lambda^*_{132}\lambda_{232}| < 1.5 \times 10^{-5}$.

In general, in most cases $\mu - e$ conversion in nuclei or $\tau \to l_iP^0$ can be used to derive even stricter limits than those given by the three-body decays. The main reason for this is the very good experimental limit due to $\mu - e$ conversion in gold and, of course, the same small dependence on the SUSY masses due to unsuppressed Z^0 penguins. This can be seen in Fig. 3. The main points of the discussion about the limits given by loop induced three-body decays also apply here. However, there is one additional, interesting observation: $\mu - e$ conversion in nuclei leads in the case of LQD couplings to a constraint for BP1, which is better than the one for BP0 by a factor of 2. This effect is larger than in the case of $l_i \to 3l_j$ decays and not only caused by the logarithmic growth of the wave function contributions. The main reason for the difference in the bounds comes from the photon contributions to $\mu - e$ conversion, which are, for BP0, of the same size as the Z^0 penguins. This leads to a negative interference reducing the severity of the limits. The very heavy squarks in the case of BP2 and BP3 are reflected by the very good limits for $\mu - e$ conversion for LQD couplings while the bounds from LLE are better for BP1 than for BP2. If the future plans to reach a sensitivity for the $\mu - e$ conversion rate in titanium of 10^{-18} [32] succeed, and no anomaly is observed, the corresponding limits are expected to improve by 3 orders of magnitude; e.g. BP2 would set a limit for $|\lambda^*_{231}\lambda_{232}|$ of 4.3×10^{-7}.

Finally, we comment on rare Z^0 decays. The flavor violating decays of the Z^0 gauge boson do not set new constraints on the parameters. In fact, for many combinations of couplings the resulting limits could only be estimated by extrapolation since they lie already in the nonperturbative regime. Only when heavy quarks are present in the loop could the Z^0 decays be of some relevance. Using the expected experimental limits of giga-Z [54], the Z^0 decays into $\mu\tau$ might reach the importance of the other observables. An estimate of the potential improvement on the bounds is shown in Fig. 4. We considered a future limit of 1.0×10^{-8} for $\mathrm{Br}(Z^0 \to \mu\tau)$ and found a limit of $O(10^{-2})$ on the product of the couplings. However, in case of lepton flavor violation in the $\mu - e$ sector, the Z^0 decays will never reach the current sensitivity of $l_i \to 3l_j$ or $\mu - e$ conversion in nuclei. To get a comparable limit,

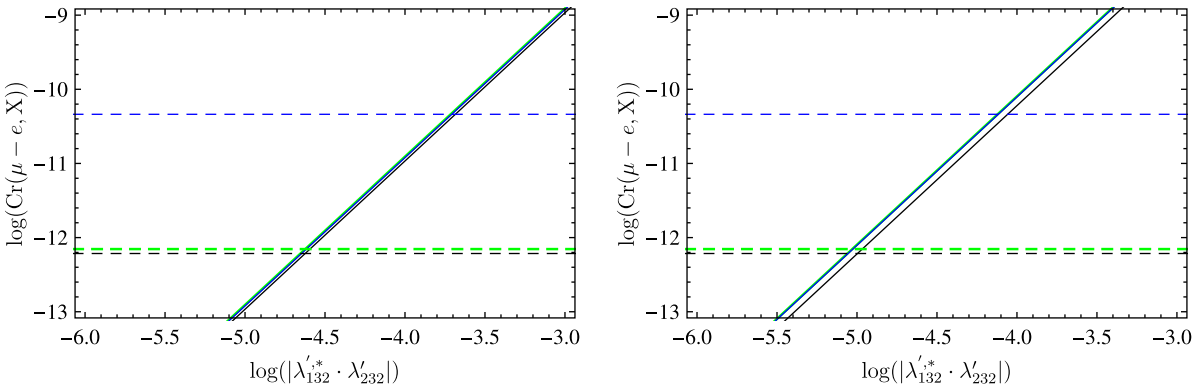

FIG. 3 (color online). $\mathrm{Cr}(\mu - e, \mathrm{Au})$ (thick solid line), $\mathrm{Cr}(\mu - e, \mathrm{Ti})$ (dotted line), and $\mathrm{Cr}(\mu - e, \mathrm{Pb})$ (thin solid line) for BP0 (left) and BP2 (right) as a function of $\log(|\lambda'^*_{132}\lambda'_{232}|)$. The current upper experimental bounds are shown by the thick dashed line (Au), the thin dashed line (Pb), and the dot-dashed line (Ti).

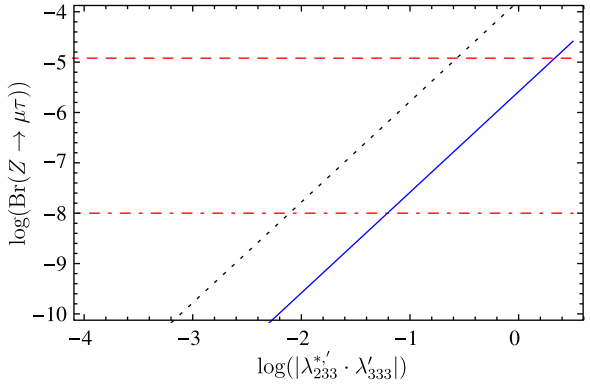

FIG. 4 (color online). $\mathrm{Br}(Z^0 \to \mu\tau)$ for BP0 (solid line) and BP1 (dotted line). The red dashed line corresponds to the current experimental Large Electron Positron Collider limit of 1.2×10^{-5} [53], and the red dot-dashed line shows the limit of 1.0×10^{-8}, which might be reached by giga-Z [54].

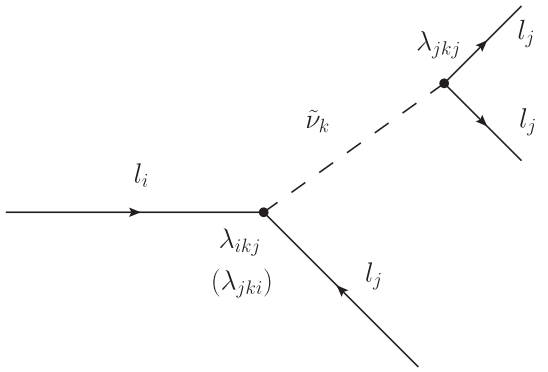

FIG. 5. Tree-level induced $l_i \to 3l_j$ decays. As shown in brackets, there are two possible combinations of λ couplings: $\lambda_{jki}\lambda_{iki}$ and $\lambda_{ikj}\lambda_{iki}$. Moreover, we remind the reader that the λ couplings are antisymmetric in the first two indices.

for instance for $|\lambda^*_{132}\lambda_{232}|$ in case of BP3 of $O(10^{-5})$, the limit of $\mathrm{Br}(Z^0 \to \mu e)$ should be improved to $O(10^{-19})$, which is far beyond the reach of the International Linear Collider with giga-Z.

V. CONCLUSION

We have considered in this paper the bounds on different combinations of LLE and LQD operators in case of trilinear R-parity violation obtained from the experimental limits on different low energy observables. We have taken into account the 1-loop induced flavor violating decays $l_i \to l_j\gamma$, $l_i \to 3l_j$, $\tau \to l_iP^0$, and $Z^0 \to l_il_j$ as well as $\mu - e$ conversion in nuclei. It turns out that the Z^0 penguins dominate in most parts of parameter space, and especially for heavy SUSY spectra, the amplitudes for $l_i \to 3l_j$, $\tau \to l_iP^0$, and $\mu - e$ conversion. Therefore, the limits on combinations of λ and λ' couplings given by these observables change only slightly between the different benchmark points. Taking into account the most stringent observables, $\mu - e$ conversion in nuclei, and $\tau \to l_iP^0$ decays, one finds for heavy SUSY scenarios improvements of several orders of magnitude with respect to the bounds already present in the literature.

ACKNOWLEDGMENTS

We thank Martin Hirsch and Werner Porod for fruitful discussions. A. V. acknowledges support from the ANR Project No. CPV-LFV-LHC NT09-508531.

APPENDIX A: TREE-LEVEL INDUCED DECAYS $l_i \to 3l_j$ AND $l_i \to l_jl_kl_k$ IN R-PARITY VIOLATION

As already mentioned, specific combinations of λ and λ' open lepton flavor violating decay channels already at tree

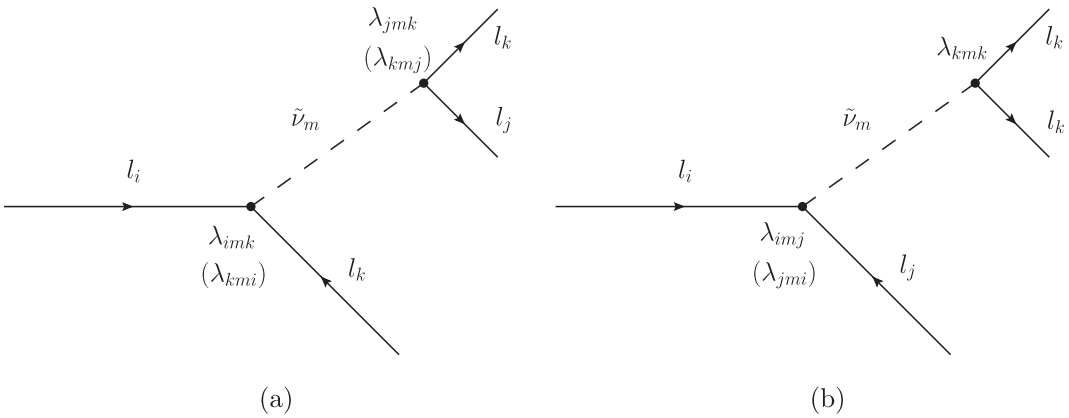

FIG. 6. Tree-level induced $l_i \to l_jl_kl_k$ decays ($j \neq k$). The different indices combinations are shown in brackets. Case (a) $\lambda_{jmk}\lambda_{imk}$, $\lambda_{jmk}\lambda_{kmi}$, $\lambda_{kmj}\lambda_{imk}$, and $\lambda_{kmj}\lambda_{kmi}$. Case (b) $\lambda_{jmi}\lambda_{kmk}$ and $\lambda_{imj}\lambda_{kmk}$. Moreover, we remind the reader that the λ couplings are antisymmetric in the first two indices.

TABLE VII. Bounds on combinations of LLE couplings from the LFV decays $l_i \to 3l_j$ and $l_i \to l_j l_k l_k$ induced at tree level.

Coupling	BP0	BP1	BP2	BP3
$\lvert\lambda^*_{121}\lambda_{122}\rvert$	5.1×10^{-7}	6.2×10^{-6}	1.9×10^{-5}	4.0×10^{-5}
$\lvert\lambda^*_{121}\lambda_{123}\rvert$	2.2×10^{-4}	2.6×10^{-3}	8.4×10^{-3}	1.7×10^{-2}
$\lvert\lambda^*_{121}\lambda_{131}\rvert$	1.7×10^{-2}	2.0×10^{-1}	2.3×10^{-1}	1.2
$\lvert\lambda^*_{121}\lambda_{132}\rvert$	1.9×10^{-2}	2.3×10^{-1}	1.5×10^{-1}	1.4
$\lvert\lambda^*_{121}\lambda_{231}\rvert$	2.2×10^{-4}	2.6×10^{-3}	8.4×10^{-3}	1.7×10^{-2}
$\lvert\lambda^*_{121}\lambda_{232}\rvert$	1.7×10^{-2}	2.0×10^{-1}	6.0×10^{-1}	1.2
$\lvert\lambda^*_{122}\lambda_{123}\rvert$	2.0×10^{-4}	2.4×10^{-3}	3.5×10^{-3}	1.5×10^{-2}
$\lvert\lambda^*_{122}\lambda_{131}\rvert$	1.9×10^{-2}	2.3×10^{-1}	2.6×10^{-1}	1.4
$\lvert\lambda^*_{122}\lambda_{132}\rvert$	2.0×10^{-4}	2.4×10^{-3}	3.5×10^{-3}	1.6×10^{-2}
$\lvert\lambda^*_{122}\lambda_{231}\rvert$	1.7×10^{-2}	2.0×10^{-1}	6.0×10^{-1}	1.2
$\lvert\lambda^*_{122}\lambda_{232}\rvert$	1.9×10^{-2}	2.3×10^{-1}	6.7×10^{-1}	1.4
$\lvert\lambda^*_{131}\lambda_{132}\rvert$	4.9×10^{-7}	6.1×10^{-6}	6.2×10^{-7}	3.1×10^{-5}
$\lvert\lambda^*_{131}\lambda_{133}\rvert$	2.2×10^{-4}	2.6×10^{-3}	2.5×10^{-4}	1.4×10^{-2}
$\lvert\lambda^*_{131}\lambda_{231}\rvert$	4.9×10^{-7}	6.1×10^{-6}	6.2×10^{-7}	3.1×10^{-5}
$\lvert\lambda^*_{131}\lambda_{233}\rvert$	1.7×10^{-2}	2.0×10^{-1}	2.0×10^{-2}	1.0
$\lvert\lambda^*_{132}\lambda_{133}\rvert$	3.5×10^{-3}	6.8×10^{-3}	2.0×10^{-2}	1.0
$\lvert\lambda^*_{132}\lambda_{233}\rvert$	1.9×10^{-2}	2.3×10^{-1}	2.3×10^{-2}	1.1
$\lvert\lambda^*_{133}\lambda_{231}\rvert$	1.7×10^{-2}	2.0×10^{-1}	2.0×10^{-2}	1.0
$\lvert\lambda^*_{133}\lambda_{232}\rvert$	1.9×10^{-2}	2.2×10^{-1}	2.3×10^{-2}	1.1
$\lvert\lambda^*_{231}\lambda_{233}\rvert$	1.9×10^{-2}	4.3×10^{-2}	2.3×10^{-2}	1.1
$\lvert\lambda^*_{232}\lambda_{233}\rvert$	2.0×10^{-4}	2.4×10^{-3}	2.3×10^{-4}	1.3×10^{-2}

level. In this context, both $l_i \to 3l_j$ and $l_i \to l_j l_k l_k$ have already been studied in detail in the literature; see, for example, Refs. [21,22]. Since several sneutrino mediated diagrams exist [see Fig. 5 (for $l_i \to 3l_j$) and Fig. 6 (for $l_i \to l_j l_k l_k$, with $j \neq k$)], quite a few combinations of $\lambda\lambda$ parameters can be constrained.

One can compute the corresponding branching ratios by means of the effective 4-fermion operator obtained after integrating out the sneutrino [21]. This possibility is perfectly valid due to the large hierarchy between the masses of the charged leptons and the mass of the sneutrino. However, we have taken a different approach, based on the exact computation of the tree-level diagrams, with full three-body phase space evaluation, including the widths of the sneutrinos.

In addition to the bounds given in Table II, we use for the tree-level decays observables with two different leptons in the final state. The experimental upper bounds on the respective branching ratios are [53]

$$\begin{aligned} \tau^- &\to \mu^- e^+ e^- : 1.8 \times 10^{-8}, \\ \tau^- &\to \mu^+ e^- e^- : 1.5 \times 10^{-8}, \end{aligned} \tag{A1}$$

$$\begin{aligned} \tau^- &\to e^- \mu^+ \mu^- : 2.7 \times 10^{-8}, \\ \tau^- &\to e^+ \mu^- \mu^- : 2.7 \times 10^{-8}. \end{aligned} \tag{A2}$$

The bounds obtained by these observables are presented in Table VII. It can be seen that the bounds for couplings that open the $\mu \to 3e$ decay mode are in agreement with [22] for BP0. All other bounds are also compatible if one considers the usual $\sim m^{-4}_{\mathrm{SUSY}}$ scaling, and in general the limits of couplings that are only sensitive to $l_i \to l_j l_k l_l$ are much weaker than those for couplings that enable also $l_i \to 3l_k$. In addition, it is interesting to see that the bounds on R pV couplings at tree level in general are not much better than those derived at 1-loop. The reason is, of course, the different scaling of the Z^0 penguin.

[1] S. P. Martin, arXiv:hep-ph/9709356.
[2] H. P. Nilles, Phys. Rep. **110**, 1 (1984).
[3] E. Gildener, Phys. Rev. D **14**, 1667 (1976).
[4] M. J. G. Veltman, Acta Phys. Pol. B **12**, 437 (1981).
[5] N. Sakai, Z. Phys. C **11**, 153 (1981).
[6] E. Witten, Nucl. Phys. **B188**, 513 (1981).
[7] J. R. Ellis, J. S. Hagelin, D. V. Nanopoulos, K. A. Olive, and M. Srednicki, Nucl. Phys. **B238**, 453 (1984).
[8] S. Chatrchyan *et al.* (CMS Collaboration), JINST **3**, S08004 (2008).
[9] G. Aad *et al.* (The ATLAS Collaboration), arXiv:0901.0512.
[10] For updated ATLAS results on SUSY searches visit https://twiki.cern.ch/twiki/bin/view/AtlasPublic/SupersymmetryPublicResults. See also https://atlas.web.cern.ch/Atlas/GROUPS/PHYSICS/CONFNOTES/ATLAS-CONF-2012-033/.
[11] For updated CMS results on SUSY searches visit https://twiki.cern.ch/twiki/bin/view/CMSPublic/PhysicsResultsSUS.
[12] L. J. Hall and M. Suzuki, Nucl. Phys. **B231**, 419 (1984).
[13] B. C. Allanach, A. Dedes, and H. K. Dreiner, Phys. Rev. D **69**, 115002 (2004); **72**, 079902(E) (2005).
[14] R. Barbier *et al.*, Phys. Rep. **420**, 1 (2005).
[15] Y. Kao and T. Takeuchi, arXiv:0910.4980.
[16] H. K. Dreiner, M. Hanussek, and S. Grab, Phys. Rev. D **82**, 055027 (2010).
[17] J. Hisano, T. Moroi, K. Tobe, and M. Yamaguchi, Phys. Rev. D **53**, 2442 (1996).
[18] E. Arganda and M. J. Herrero, Phys. Rev. D **73**, 055003 (2006).
[19] K. S. Babu and C. Kolda, Phys. Rev. Lett. **89**, 241802 (2002).
[20] M. Hirsch, F. Staub, and A. Vicente, arXiv:1202.1825.

[21] D. Choudhury and P. Roy, Phys. Lett. B **378**, 153 (1996).
[22] A. de Gouvea, S. Lola, and K. Tobe, Phys. Rev. D **63**, 035004 (2001).
[23] H. K. Dreiner, M. Kramer, and B. O'Leary, Phys. Rev. D **75**, 114016 (2007).
[24] E. Lunghi, A. Masiero, I. Scimemi, and L. Silvestrini, Nucl. Phys. **B568**, 120 (2000).
[25] A. Schöning, S. Bachmann, and R. Narayan, Phys. Procedia **17**, 181 (2011).
[26] A. Ilakovac and A. Pilaftsis, Nucl. Phys. **B437**, 491 (1995).
[27] E. Arganda, M. J. Herrero, and A. M. Teixeira, J. High Energy Phys. 10 (2007) 104.
[28] E. Arganda, M. J. Herrero, and J. Portoles, J. High Energy Phys. 06 (2008) 079.
[29] C. Dohmen *et al.* (SINDRUM II Collaboration), Phys. Lett. B **317**, 631 (1993).
[30] W. Honecker *et al.* (SINDRUM II Collaboration), Phys. Rev. Lett. **76**, 200 (1996).
[31] W. H. Bertl *et al.* (SINDRUM II Collaboration), Eur. Phys. J. C **47**, 337 (2006).
[32] R. M. Carey *et al.* (Mu2e Collaboration), Report No. FERMILAB-PROPOSAL-0973.
[33] Y. G. Cui *et al.* (COMET Collaboration), Report No. KEK-2009-10.
[34] M. Chemtob and G. Moreau, Phys. Rev. D **59**, 116012 (1999).
[35] J. M. Yang, Sci. China: Phys., Mech. Astron. **53**, 1949 (2010).
[36] X. J. Bi, Y. B. Dai, and X. Y. Qi, Phys. Rev. D **63**, 096008 (2001).
[37] G. Bhattacharyya, Nucl. Phys. B, Proc. Suppl. **52**, 83 (1997).
[38] B. C. Allanach, A. Dedes, and H. K. Dreiner, Phys. Rev. D **60**, 075014 (1999).
[39] H. K. Dreiner, G. Polesello, and M. Thormeier, Phys. Rev. D **65**, 115006 (2002).
[40] V. D. Barger, G. F. Giudice, and T. Han, Phys. Rev. D **40**, 2987 (1989).
[41] T. Banks, Y. Grossman, E. Nardi, and Y. Nir, Phys. Rev. D **52**, 5319 (1995).
[42] M. Hirsch and J. W. F. Valle, New J. Phys. **6**, 76 (2004).
[43] A. Faessler, T. S. Kosmas, S. Kovalenko, and J. D. Vergados, Nucl. Phys. **B587**, 25 (2000).
[44] W. Porod, Comput. Phys. Commun. **153**, 275 (2003).
[45] W. Porod and F. Staub, arXiv:1104.1573.
[46] F. Staub, T. Ohl, W. Porod, and C. Speckner, arXiv:1109.5147.
[47] F. Staub, Comput. Phys. Commun. **182**, 808 (2011).
[48] F. Staub, Comput. Phys. Commun. **181**, 1077 (2010).
[49] T. Hahn, Comput. Phys. Commun. **140**, 418 (2001).
[50] T. Hahn, Proc. Sci., ACAT08 (2008) 121.
[51] S. S. AbdusSalam *et al.*, Eur. Phys. J. C **71**, 1835 (2011).
[52] J. Adam *et al.* (MEG Collaboration), Phys. Rev. Lett. **107**, 171801 (2011).
[53] K. Nakamura *et al.* (Particle Data Group), J. Phys. G **37**, 075021 (2010).
[54] J. I. Illana, M. Jack, and T. Riemann, in "2nd ECFA/DESY Study 1998-2001," pp. 490–524.